Polymer Chemistry

ROYAL SOCIETY OF CHEMISTRY

PAPER

View Article Online
View Journal | View Issue

Cite this: *Polym. Chem.*, 2025, **16**, 181

Converting high modulus water-based elastomeric core–shell nanoparticle films from viscoelastic to predominantly elastic using di-epoxide crosslinking†

Mollie Osborne-Richards, *[a] David Ring,[b] Xuelian Wang,[a] Sarah Wall,[a] Steve Edmondson [a] and Brian R. Saunders *[a]

Most elastomers are formed using solvent-based processes which result in an environmental burden. Consequently, elastomers formed using water-based nanoparticle dispersions are highly desirable. Here, we investigate elastomer-like films based on water-dispersible carboxylic acid-containing core–shell (CS) nanoparticles. The nanoparticles contain a poly(*n*-butylacrylate) (PBA) core and a poly(BA-*co*-acrylonitrile-*co*-methacrylic acid) shell. We react the –COOH groups of the shell with a di-epoxide (1,4-butanediol diglycidyl ether, BDDE) which replaces dissipative hydrogen bonds in the nanoparticle elastomer films with covalent bonds. The reaction with BDDE enables the transformation of a stretchable dissipative film (shear modulus of 9.0 MPa with 20% strain energy recovery) into a predominantly elastic film (shear modulus of 0.20 MPa with almost 100% energy recovery). Our optimum system, CS-0.5, has a shear modulus of 0.40 MPa, an impressive strain-at-break of greater than 300% and an energy recovery of 80%. The strain-at-break is increased to more than 450% using a monofunctional epoxide. We further explore the inter- and intra-nanoparticle nature of the di-epoxide reaction and how the mechanical properties can be tuned by varying the method of film formation. The facile approach introduced here enables the tuning of the mechanical properties of elastomeric core–shell nanoparticle films from dissipative to predominantly elastic on demand.

Received 24th September 2024,
Accepted 24th November 2024

DOI: 10.1039/d4py01073f

rsc.li/polymers

Introduction

Elastomer materials are crosslinked polymers that can be stretched by significant elongation and then return to their original size with little to no permanent deformation.[1–3] The term elastomer usually refers to a fully crosslinked network. If there is incomplete crosslinking then, strictly, the material will be viscoelastic. Elastomer materials are used for a wide range of applications as they can be adhesive,[4–6] strong,[7] stretchable[8–10] and moldable.[11,12] Therefore, the characteristics of elastomers need to be easily tuneable for the desired application.[13,14] A common method for preparing elastomers is by solution processing; however, this process often uses harmful solvents[8,15] which are released as volatile organic compounds into the atmosphere and raise environmental concerns.[16–18] Consequently, there is an urgent need to develop more environmentally friendly elastomer syntheses.[19] The present study demonstrates a new water-based synthesis for preparing high modulus, core–shell (CS) nanoparticle elastomer-like films with highly tuneable mechanical properties that are shown to be controllable *via* nanoparticle composition, nanoparticle crosslinking and film preparation methods.

Elastomers are crosslinked by either physical crosslinking or chemical crosslinking.[20] Common crosslinking strategies employ covalent bonding[21,22] and hydrogen bonding,[20,23,24] with dynamic bonding (including disulfide bonding[25,26]) coming into the spotlight in recent years.[21,27,28] To create more environmentally friendly elastomers, solvents are being replaced with water-based dispersions that form elastomeric films.[29–35] For such systems, the elastomeric film is formed as the water evaporates and the particles deform. Interpenetration then occurs at the particle–particle interface, causing coalescence.[15,31] To improve the mechanical properties of such films, *inter*-particle, physical crosslinking can be introduced by the addition of hydrogen bonding or ionic interactions.[16,31,36]

[a]*Department of Materials, University of Manchester, MECD(A), Manchester, M1 7HL, UK. E-mail: brian.saunders@manchester.ac.uk, mollie.osborne-richards@postgrad.manchester.ac.uk*
[b]*Synthomer (UK) Ltd, Temple Fields, Harlow, Essex, CM20 2BH, UK*
† Electronic supplementary information (ESI) available. See DOI: https://doi.org/10.1039/d4py01073f

Additionally, CS nanoparticles are advantageous for film property control because the core and the shell can be separately modified to tune elastomer mechanical properties.[37–39] They have been studied extensively for a range of applications from semiconductors[40,41] to drug delivery.[42,43] Crucially, CS nanoparticles have been investigated as sustainable alternatives to solvent-based polymer films.[31,35,44,45] The core of the CS nanoparticles is usually synthesized first followed by addition of the shell which forms around the core *in situ*[43] as a uniform layer.[46] The properties of both the core and the shell can be separately tailored, resulting in versatile CS nanoparticles.[46,47]

Previously we investigated the nanostructure of elastomeric films based on CS nanoparticles with a poly(*n*-butyl acrylate) (PBA) core and a shell containing a copolymer of BA, acrylonitrile (AN), methacrylic acid (MAA) and 1,4-butanediol diacrylate (BDDA).[37] The *inter*-particle crosslinking in those PBA/(PBA–AN–MAA–BDDA) nanoparticle films was from hydrogen bonds and free-radical coupling of vinyl groups that occurred when the films were heated. The film's mechanical properties were tunable *via* the MAA content and/or the extent of vinyl-based *inter*-particle crosslinking.[48,49] Unfortunately, the versatility of that approach was hindered by the oxygen-triggered radical crosslinking reaction that inevitably occurred at the high temperatures required for vinyl crosslinking.[37] In contrast, here we introduced a new CS dispersion preparation method coupled with a low-temperature crosslinking method that uses a *non*-free-radical di-epoxide reaction. The di-epoxide will crosslink across polymer chains within the shell of the particles as the ring opens and reacts with the –COOH groups. We hypothesized that the CS elastomer-like films would have profound mechanical property tuneability whilst maintaining high elongation-at-break.

In this study, we sought to establish a facile method for covalently interlinking CS nanoparticle films using 1,4-butanediol diglycidyl ether (BDDE) added to the nanoparticle dispersion (Scheme 1). The di-epoxide is shown to act as a crosslinker and change the properties of the CS-*x* films *via* two-stage *intra*- and *inter*-particle reactions (*x* is the mass of BDDE added in g). In the first stage (Stage I, *pre*-film casting) BDDE is reacted with the –COOH groups. Excess BDDE remains after Stage I and subsequently reacts during elastomer film formation (Stage II, *post*-film casting). This method dramatically changes the mechanical properties of the CS nanoparticle films, transforming them from dissipative to predominantly elastic films. All the films in the study are viscoelastic materials. We show that the extent of elastic behaviour is highly tunable *via* the BDDE concentration used. We separately

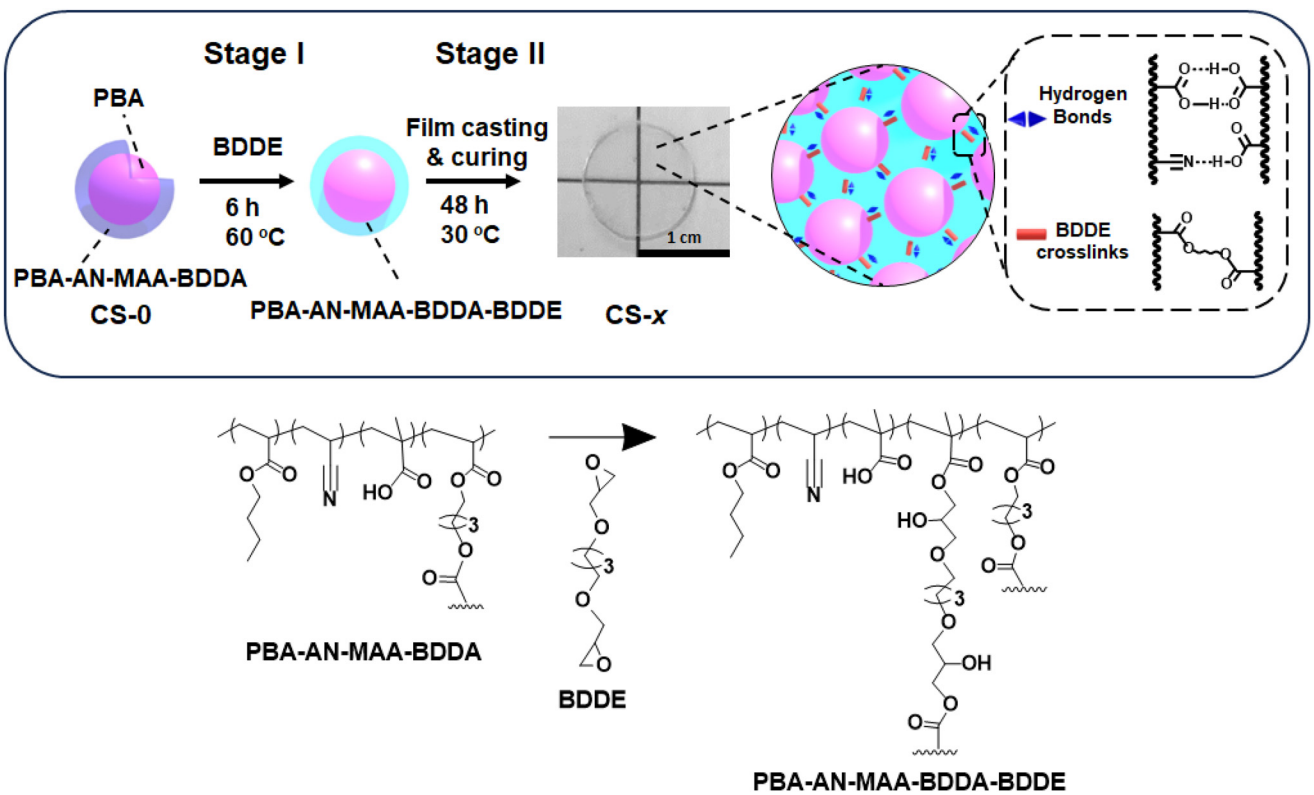

Scheme 1 Depiction of the formation of CS-*x* films (*x* is the mass of BDDE added in g) after the first pre-film casting reaction with BDDE (Stage I) followed by the post-casting reaction during film formation (Stage II). Stages I and II indicate the two stages of reaction of BDDE with the –COOH functional groups of the particles. BA, AN, MAA and BDDA are *n*-butylacrylate, acrylonitrile, methacrylic acid and 1,4-butanediol diacrylate, respectively. BDDE is 1,4-butanediol diglycidyl ether. The reaction of some of the –COOH groups in the PBA–AN–MAA–BDDA shell with BDDE gives additional covalent crosslinking (depicted).

investigate the contributions from Stage I and Stage II reactions on the final film mechanical properties by isolating the contributions from each stage. We demonstrate that the greatest change in mechanical and elastic properties of the films occurs when both Stage I and II reactions occur. This study provides a new and scalable water-based method to tune the mechanical properties of nanoparticle-based elastomer films.

Results and discussion

Core–shell nanoparticle reaction with BDDE during the pre-film casting stage (Stage I)

The as-made parent CS nanoparticles (denoted as CS-0) were prepared by semi-batch emulsion polymerization (Scheme S1†) as described in the Experimental section using a method inspired by a microgel study.[50] The growth of the CS-0 nanoparticles was monitored by dynamic light scattering (Fig. S1a†) and gravimetric measurements. The constant number of particles (N_P, Fig. S1b†) showed that there was no secondary nucleation (see Additional Note 1†). We reacted the CS-0 nanoparticles with increasing masses of BDDE in the dispersion as depicted in Scheme 1 (Stage I) to prepare CS-*x* nanoparticles. The reaction of the –COOH groups with BDDE is necessarily *intra*-particle in nature at this *pre*-film casting stage (*i.e.*, Stage I, Scheme 1). The number-average diameters of the nanoparticles (106–109 nm) are not affected by addition of BDDE (Fig. 1a–d) and the nanoparticles are spherical with a standard deviation of <15 nm (Fig. S2 and Table S1†). The nanoparticle dispersions were analyzed by potentiometric titration (Fig. S3†) which gave the MAA concentration (wt%) and pK_a value of each sample (Fig. 1e and Table S1†). As the mass of BDDE (x) added during the reaction increases, more epoxide reacted with the –COOH groups, reducing the MAA concentration in the nanoparticles. The pK_a of the nanoparticles increased as the MAA concentration decreased in line with earlier reports for related nanoparticles.[51] From the titration data, the percentage of –COOH groups that reacted with BDDE during Stage I was calculated (Fig. S4†). This value increased from 8.5% for the CS-0.25 system to 21.3% for the CS-1 system. Consequently, there was unreacted "free" BDDE present after Stage I. We show below that this *free* BDDE subsequently reacted during film formation (Stage II in Scheme 1). Because there are two stages of BDDE reaction, we term films prepared using both the *pre*-film casting and *post*-film casting reactions as Stage I + II films. The CS-*x* nanoparticles are pH responsive as shown in Fig. 1f. Whilst the d_z value for the initial CS-0 sample increased from 100 to 125 nm as the pH increased from 4 to 10, the reaction of BDDE with the nanoparticles *decreased* the pH response. Indeed, the nanoparticles with the highest proportion of –COOH reacted (*i.e.*, CS-1) only swelled to 107 nm at pH 10. The decrease in swelling with increasing x at pH 10 is shown in Fig. 1g. The data for pH 10 and pH 4

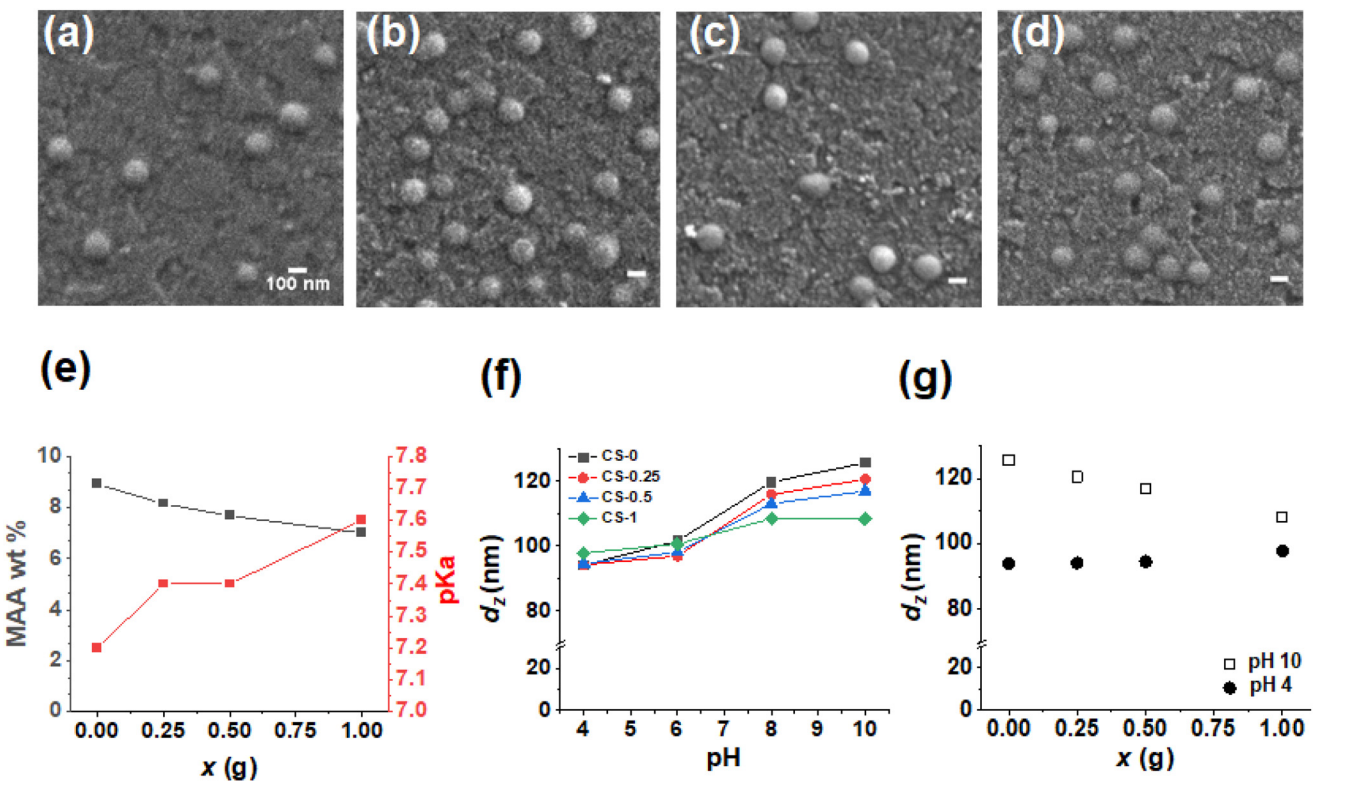

Fig. 1 SEM images of (a) CS-0, (b) CS-0.25, (c) CS-0.5 and (d) CS-1 nanoparticles deposited from water. Scale bars: 100 nm. (e) Concentration of MAA wt% in the CS-*x* nanoparticles and their pK_a values. (f) Measured *z*-average diameters of the nanoparticles at different pH values. (g) Data from (f) at pH 4 and pH 10 plotted as a function of *x*.

approach convergence as x increases. This decrease in swelling is due to the BDDE reacting with the RCOOH and is a key indicator of the crosslinking reaction, depicted in Scheme 1. Furthermore, the nanoparticles become more negatively charged with the increase in the pH due to $-COO^-$ formation, with the zeta potential increasing to ~ −40 mV (Fig. S5†) at pH 10.0 compared to ~ −20 mV at pH 4.0. Taken together, these data confirm that –COOH groups remain for all the CS-x systems after the Stage I reaction.

Analysis of Stage I + II films cast from dispersions containing reacted and free BDDE

Stage I + II films were prepared by casting CS-x dispersions at 30 °C for 48 h. The dispersions used contained CS-x nanoparticles that had partially reacted with BDDE, as well as free BDDE in the continuous phase (Scheme 1). This method resulted in thin transparent films (Fig. 2a). The films prepared in this way contained less than 1 wt% residual water as judged by thermogravimetric analysis for a CS-0.5 film (Fig. S6†). To investigate the effect the crosslinking had on the film surface topology, the films were studied using AFM (Fig. S7†). Individual nanoparticles can be discerned for CS-0. However, irregularly shaped features are seen on the surface of the CS-x films which indicates that extensive coalescence of nanoparticles occurred as the films formed, which is due to their lower glass transition temperature (T_g) values (discussed below).

Based on the DLS data (Fig. S1†), the core and shell of the CS-0 nanoparticles occupy ~34% and 66% of the particle volume, respectively. We envisage the morphology depicted in the top right of Scheme 1 wherein soft PBA cores are dispersed within a continuous phase of inter-meshed (coalesced) nanoparticle shells. Accordingly, the mechanical properties of the CS-x films result directly from those of the constituent nanoparticles. We have shown previously[48] that the mechanical properties of this general type of core–shell film can be described by the isostrain model[52] for biphasic gels. In the present case, a soft PBA core is dispersed within a relatively hard PBA–AN–MAA–BDDA–BDDE (shell) matrix. In such a model, the shear modulus (G) for the CS-x film is the volume fraction weighted sum of that from the core and shell parts of the constituent nanoparticles. Because of the dominance of the shell volume fraction and their likely relatively high G values, we assume

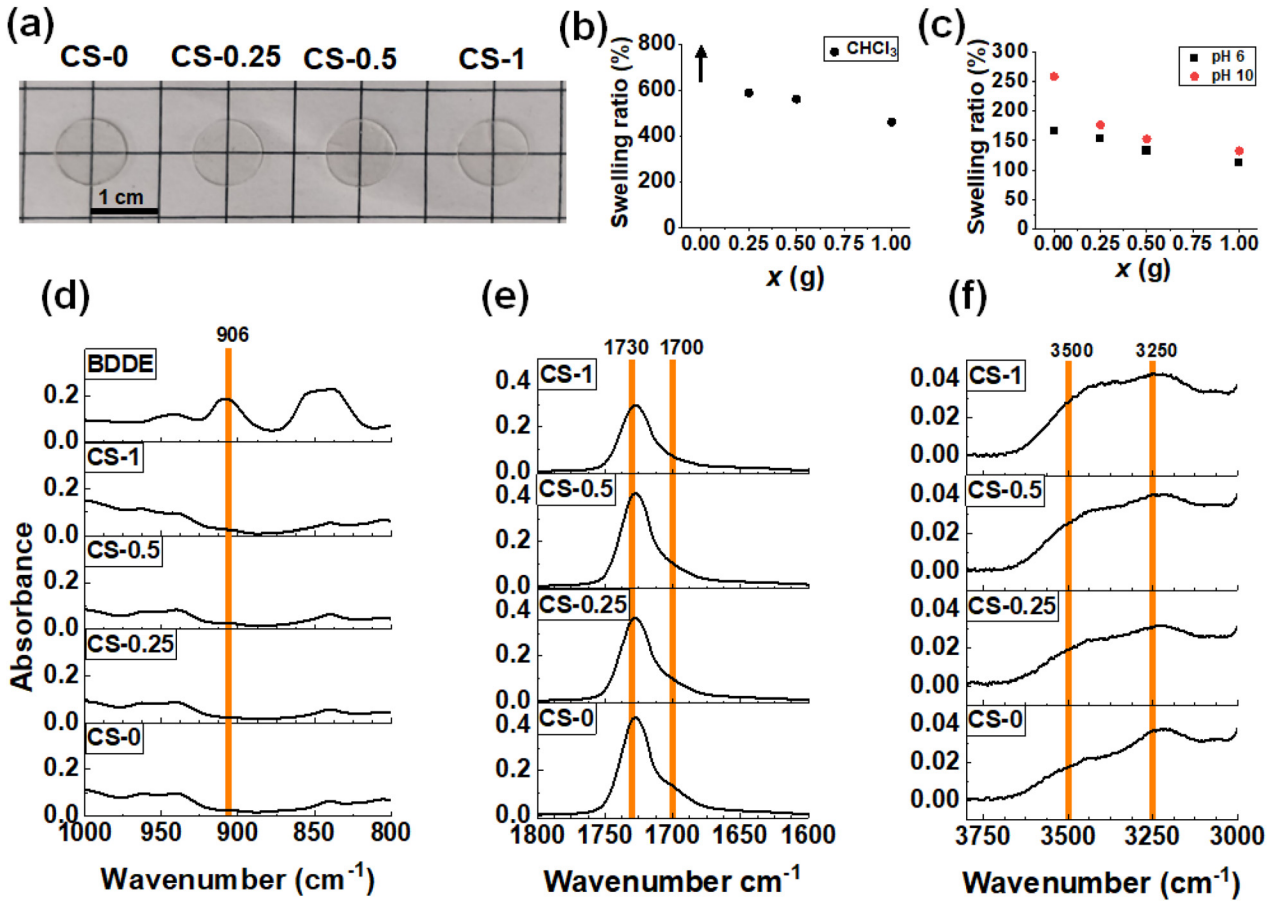

Fig. 2 (a) Photographs of each of the Stage I + II films (thickness = 0.5 mm). (b) The swelling ratios of the films in $CHCl_3$ after 5 days. The arrow shows that the CS-0 film, which swelled considerably, became too brittle to measure. (c) Swelling ratio of the films in water at pH 6 and 10. Expanded views of the FTIR spectra for the (d) epoxide region, (e) C═O region and (f) –OH region (see the text).

that the G values for the present systems are dominated by that of the nanoparticle shells.

We conducted swelling tests in $CHCl_3$ (Fig. S8a†) as well as in water at pH 6 and pH 10 to probe crosslinking changes in the CS-x films.[53] Unlike the CS-0 film which swelled to the point of dissolution in $CHCl_3$, the CS-x films exhibited good tolerance to $CHCl_3$, as evidenced by the finite mass swelling ratios (Fig. 2b). As x increased, the swelling ratio of the films decreased, indicating that crosslinking occurred between the polymer chains due to the reaction with BDDE. The films were also immersed in water at pH 6 (Fig. S8b†) and pH 10 (Fig. S8c†). The swelling ratios for the CS-x films (Fig. 2c) decreased as x increased, again indicating that higher crosslinking occurred at higher x values. Lower –COOH contents in the higher x films likely also contributed to less swelling. The swelling ratios are higher in pH 10 water than in pH 6 water which shows that unreacted $–COO^-$ groups drive the swelling of these films at pH 10. These data are consistent with the DLS data (Fig. 1f) and support our view that the Stage I + II CS-x films contained both –COOH groups and covalent crosslinks due to the reaction of some of the original –COOH groups with BDDE.

FTIR spectra for each film were measured (Fig. S9a†). The BDDE spectrum has a peak at 906 cm^{-1} due to the epoxide[54–56] which is not present in the spectra for the CS-x films (Fig. 2d). Scrutiny of these signals in the epoxide region (Fig. 2d) confirms that the *epoxy has reacted after CS-x film formation*. Thus, by the end of Stage II there is no detectable unreacted BDDE. As x is increased in the CS-x films and –COOH reacts with the epoxide, changes are seen in the C═O region of the FTIR spectra (Fig. 2e). As the amount of –COOH that reacts increases with x, using up hydrogen bonding sites, the shoulder peak at 1700 cm^{-1} (which is due to –COOH) decreases (Fig. 2e). This is shown in Fig. S9b† where the absorbance ratio of the 1700 cm^{-1} shoulder to the sum of the 1700 cm^{-1} shoulder and the 1730 cm^{-1} ester peak[57] is plotted. Additionally, as the –COOH group reacts and opens the epoxy ring (Scheme 1), a shifting peak is identified in the –OH spectral region (Fig. S9a†) which is expanded in Fig. 2f. The CS-0 film has a broad –OH peak at 3250 cm^{-1}, whereas upon reaction of –COOH with the epoxide, a new –OH bond[58] is formed at 3500 cm^{-1}, which grows as x increases and is plotted in Fig. S9c† as a function of x. Consequently, the FTIR spectra show that *reaction between the –COOH groups and epoxide groups occurred*. Hence, less hydrogen bonding occurred in the films as x increased due to the ring-opening reaction of BDDE with –COOH and covalent bond formation (Scheme 1).

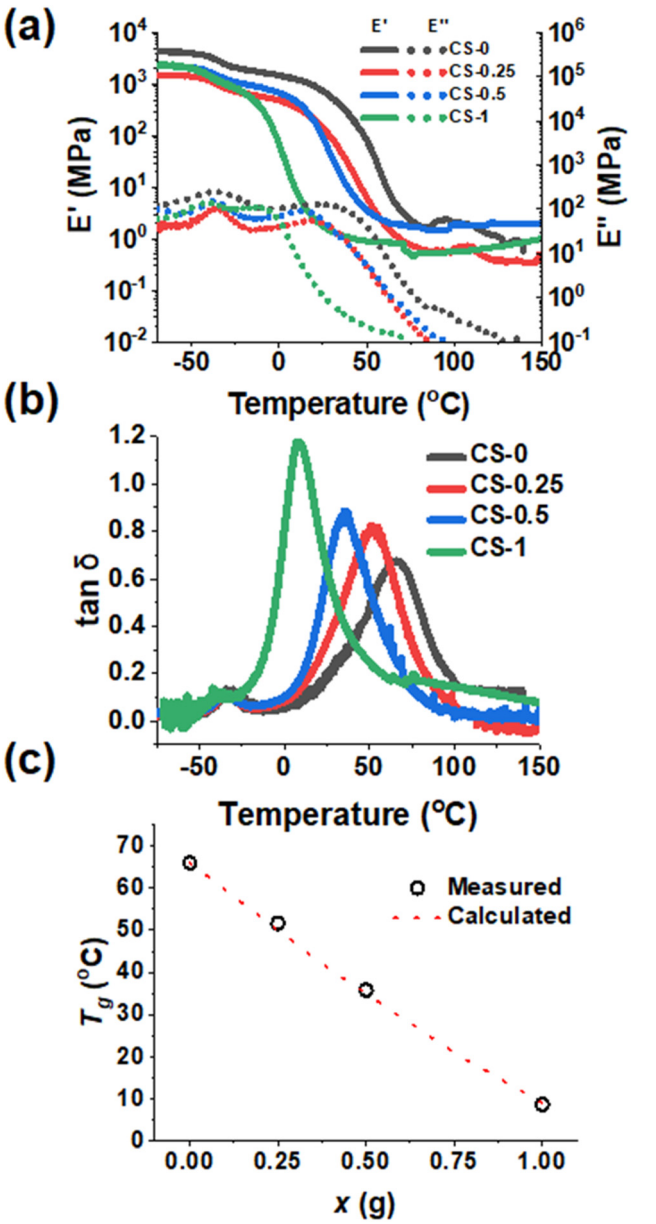

Fig. 3 (a) Storage modulus (E') and loss modulus (E'') from representative DMA measurements *versus* temperature. (b) Variation of representative tan δ (= E''/E') as a function of temperature for the films. (c) Glass transition temperature (T_g) of each film sample measured using the main peak of the tan δ *versus* temperature data shown in (b) compared to the calculated T_g using the Fox equation.

Mechanical properties of the Stage I + II films

To examine the mechanical properties of the CS-x films as a function of temperature, DMA data were measured to obtain the storage (E') and loss (E'') modulus and tan δ = (E''/E') values. The E' values show strong temperature dependencies (Fig. 3a) and decrease by several orders of magnitude as the temperature increases from −70 °C. This is due to the glass transition temperature (T_g) of the PBA core and, subsequently, the PBA–AN–MAA–BDDA shells of the nanoparticles being exceeded as the temperature increases. Moreover, there is a strong decrease in E' between 0 and 25 °C with increasing x. Hence, the reaction with BDDE strongly decreases film stiffness at room temperature. Furthermore, as the temperature increases above 100 °C, the E' values show increasingly plateau-like behaviour which is most pronounced for the Cs-x films with $x \geq 0.5$. Such higher temperature E' plateaus are indicative of elastic behaviour.

The peak of the tan δ *versus* temperature data (Fig. 3b) is indicative of the T_g.[59,60] Fig. 3b shows two peaks that correspond to T_g values. The lower temperature peak at ~ −40 °C is from the PBA core of the CS-*x* nanoparticles.[37,60] This peak is consistent with soft PBA nanoparticle cores dispersed within a harder inter-meshed shell matrix as depicted in Scheme 1. The core T_g did not change as x increased, showing that shell crosslinking does not affect chain mobility in the core. The tan δ peak which occurs in a temperature range from 0 °C to 70 °C is attributed to the shell of the nanoparticles.[37] An increase in x caused a decrease in these T_g values (Fig. 3c). We applied the Fox equation for predicting poly(A-*co*-B) copolymer glass transition temperature values (equation (S2), Additional Note 2†) to our present systems.[61] The results from the Fox equation are shown in Fig. 3c. The agreement between the measured and calculated T_g values for the x = 0.25 and 0.5 systems is remarkably good. It follows that the reaction with BDDE (which governs the T_g) occurs uniformly throughout the shells of these core–shell nanoparticles and that such copolymer shells form a well-mixed continuous phase within the final nanoparticle films.

The addition of a crosslinker would normally be expected to increase the T_g of an elastomer[62] and so the present trend from Fig. 3c appears counterintuitive at first sight. However, as BDDE reacted, the amount of –COOH available for inter-chain hydrogen bonding in the film decreased. This decrease of inter-chain hydrogen bonding (and dynamic crosslinks) increased chain mobility. Whilst covalent crosslinks were produced by the BDDE reaction, their effect on the T_g appears to have been overwhelmed by the decrease in hydrogen bonding between –COOH groups, decreasing the T_g.

The CS-*x* films underwent tensile testing and show distinctive changes as x is increased (Fig. 4a). (Tensile data for all systems appear in Table S2.†) When x = 0, there was initial elastic deformation followed by plastic deformation as the modulus drops beyond the first 20% strain. As x increased, the effect of plastic deformation dramatically decreased, leaving elastic deformation as the dominating effect. We assume that hydrogen bonds involving –COOH are responsible for the plastic deformation. The shear modulus of the films (Fig. 4b) falls from 9.0 MPa when x = 0 to 1.1, 0.40 and 0.20 MPa for the CS-0.25, CS-0.5 and CS-1 films, respectively. The stress-at-break decreased strongly with the increase in x (Fig. 4c), while the strain-at-break (Fig. 4d) remained high (>300%) for the CS-*x* films when x = 0, 0.25 and 0.5, before decreasing to a respectable value of 142% for the CS-1 film. For these CS-*x* nanoparticle elastomer-like films, the modulus is considered to reflect *intra*-particle crosslinking, and the strain-at-break reflects *inter*-particle crosslinking.[48] The decrease in strain-at-break for the CS-1 system (Fig. 4d) is attributed to a major change from dissipative hydrogen bonding to non-dissipative covalent *inter*-particle crosslinking which can accommodate less fracture energy.[63–65] In contrast, the CS-*x* systems with $x \leq$ 0.5 had more –COOH groups that could dissipate strain *via* dynamic hydrogen bonds and, therefore, retained higher strain-at-break values.

Cyclic tensile measurements were performed to provide greater insight into the CS-*x* film mechanical properties (Fig. 4e and f). For CS-0, the steep increase in tensile stress corresponds to the initial elastic deformation which then yields with plastic deformation. This yielding caused the

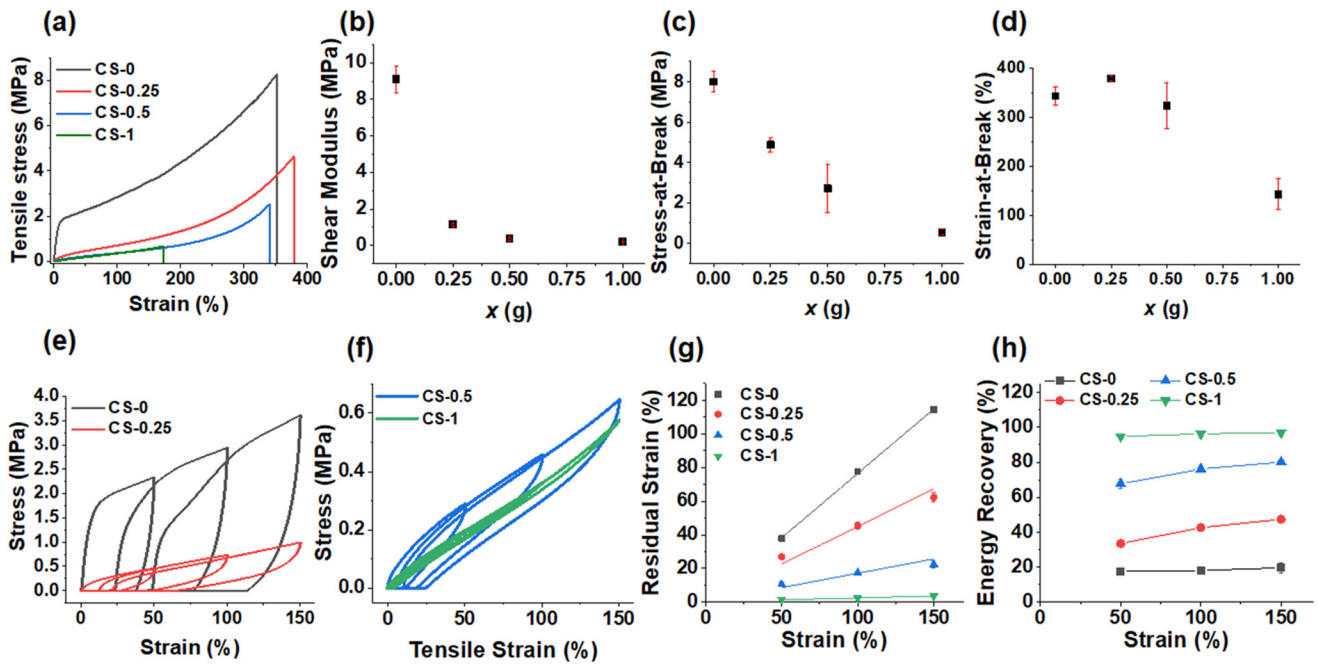

Fig. 4 (a) Representative tensile stress/strain data for the Stage I + II films. The (b) shear modulus, (c) stress-at-break and (d) strain-at-break are shown for each system. Representative cyclic tensile data are shown for (e) CS-0 and CS-0.25 as well as (f) CS-0.5 and CS-1.0. The (g) residual strain values and (h) energy recovery values measured at each final tensile strain from (e) and (f) are shown.

material to deform irreversibly, and thus, not return to 0% strain when the stress was removed. When $x > 0$, the amount of irreversible deformation for the CS-x films decreased. The residual strain values measured from Fig. 4e and f are plotted in Fig. 4g and increase linearly with tensile strain. The residual strain values at 150% dramatically decrease from ~115% to less than 5% as x increases from 0 to 1.0 revealing greatly increased elasticity.

When comparing the energy recovery data (calculated from the area ratio of the reverse to forward stress *vs.* strain sweeps in Fig. 4e and f), the energy recovery at all applied strains (Fig. 4h) increased from ~20% for CS-0 to 97% for CS-1. The trends shown in Fig. 4g and h demonstrate a major change from sacrificial –COOH-based crosslinking to covalent (permanent) crosslinking for the CS-x films when x increases from 0 to 1.0. Hence, the reactions of the nanoparticles with BDDE transform the dissipative predominantly viscoelastic CS-0 film into a predominantly elastic CS-1 film. Whilst these films are all viscoelastic materials, the contribution of the viscous component to the overall mechanical properties decreases with increasing x. The CS-0.25 and CS-0.5 films contain mixtures of dynamic crosslinks (from –COOH) and covalent crosslinks (from –COOH plus di-epoxide reaction). In particular, the CS-0.5 system is noteworthy because it has a high modulus (0.40 MPa), high strain energy recovery (80%) and high strain-at-break (323%).

We inferred above from the titration data (Fig. S3†) and the formulations used to prepare these films that (a) free BDDE was present after the Stage I reaction (Scheme 1) and (b) from the FTIR data (Fig. 2b) that free BDDE was consumed during Stage II. A key question concerns the importance of the BDDE reactions during Stage I and Stage II for the dramatic (and tuneable) mechanical property changes observed in Fig. 3 and 4. We address this question in the next section.

The Stage I reaction occurred in the dispersed state and was conducted at 60 °C for 6 h. The Stage II reaction was conducted at 30 °C for 48 h and also began in the dispersed state. We propose that the reactions that occurred in Stages I and II were broadly similar at the molecular level. If the Arrhenius rule of thumb that the reaction rate doubles when the temperature increases by 10 °C is applied to the present systems, it follows that the Stage I and Stage II reactions used are equivalent in terms of the extent of reaction. (Stage II may have occurred at a rate that was eight times slower but the duration was eight times longer than Stage I.) However, the transformation of a dispersion into a dry film of coalesced particles that is unique to Stage II would likely affect the reaction kinetics in that stage. It is plausible that a significant part of the BDDE reaction occurred after extensive nanoparticle coalescence had taken place.

Mechanical properties of Stage I films cast from dispersions without free BDDE

To investigate the effect of the Stage I reaction, a CS-1 dispersion was dialyzed against water for 5 days prior to film formation (depicted in Fig. 5a) to remove unreacted (free) BDDE. These Stage I films are denoted CS-1-D. Notably, the DMA data (Fig. 5b) show that the peak of CS-1-D has a much *higher* T_g (57 °C) than measured for the (Stage I + II) CS-1 film (9 °C, Fig. 3c). The T_g is also 10 °C *lower* than that for the CS-0 film (67 °C, Fig. 3c). The tensile data (Fig. 5c) show that the CS-1-D film has less plastic deformation than the CS-0 film but more than the CS-1 film. The modulus of CS-1-D (5.0 MPa) is much lower than that of the CS-0 system (9.0 MPa) but much higher than that of CS-1 (0.20 MPa) (Fig. 5d). The stress-at-break values (Fig. 5e) for the CS-1-D film is in between those of the CS-0 and CS-1 films. As it was established above that the BDDE reaction decreases the T_g, modulus and stress-at-break, the data for CS-1-D reveal that a significant reaction of BDDE occurred during Stage I of the CS-1 film, prepared using the Stage I + II method. Furthermore, if the Stage I reaction (Fig. 5a) was exclusively *intra*-particle in nature, then one would expect that the strain-at-break, which is dominated by *inter*-particle crosslinks, would be unaffected. This suggestion is confirmed by the strain-at-break value for CS-1-D of 318% which is very close to that for CS-0 (330%, Fig. 5f).

Cyclic tensile data for the CS-1-D film also show a plastic yield point and the data appear closer to CS-0 than to CS-1 in behavior (Fig. 5g). Notably, the residual strain (Fig. 5h) and energy recovery (Fig. 5i) at each strain measured are close to the values observed for the CS-0 film. These data confirm the dissipative nature of the CS-1-D films which is due to the dominance of reversible –COOH crosslinks in the nanoparticle shells. It follows from the Stage I CS-1-D film data discussed here that for the CS-1 film prepared using the Stage I + II method, free BDDE and the Stage II reaction are vital to fully develop the dissipative-to-elastic transition achieved for the CS-x films.

Mechanical properties of Stage II films cast from dispersions containing added BDDE

An interesting question arising from the Stage I CS-1-D film data discussed above is whether simply using a Stage II reaction *only* can achieve the pronounced mechanical property changes observed for the CS-x (x = 0.25, 0.5, 1.0) films shown in Fig. 3 and 4. Accordingly, we studied films prepared using the Stage II process only. These films were formed by addition of BDDE to a CS-0 dispersion *without* a Stage I reaction (Fig. 6a). This system is denoted as CS-0 + BDDE. The masses of BDDE and CS-0 nanoparticles used were the same as those used to prepare the CS-1 film using the Stage I + II process (Scheme 1). From the DMA data for the CS-0 + BDDE film (Fig. 6b), the T_g of the film is 41 °C. This is much higher than that for the CS-1 film (9 °C). The T_g is also considerably lower than that for CS-0 (67 °C, Fig. 3c). These data show that a substantial proportion of the –COOH groups reacted with BDDE during the Stage II process.

Tensile data comparing CS-0 + BDDE with CS-0 and CS-1 are shown in Fig. 6c. The plastic deformation seen for the CS-0 film is present for the CS-0 + BDDE film. Furthermore, the CS-0 + BDDE modulus (Fig. 6d) is in between those of CS-1 and CS-0 while the stress-at-break (Fig. 6e) value is closer to that of CS-0 than that of CS-1. Interestingly, the strain-at-break

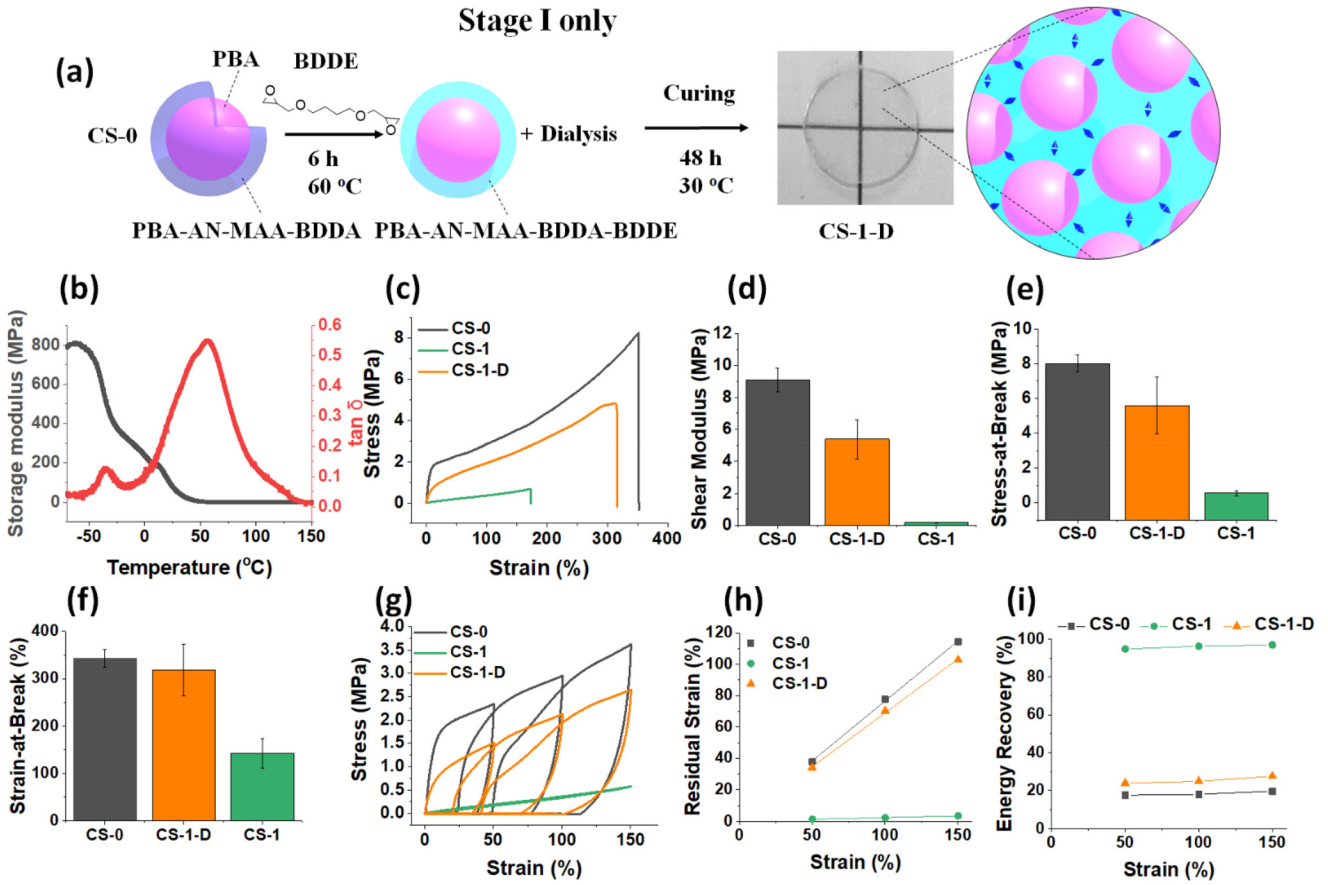

Fig. 5 (a) Depiction of the formation of CS-1-D films where the CS-1 dispersion is dialyzed to remove residual BDDE prior to film formation. The CS-1-D films have only the Stage I reaction with BDDE. (b) Variation of E' and tan δ with temperature measured for the CS-1-D film. (c) Representative stress–strain curve of CS-1-D compared to CS-0 and (Stage I + II) CS-1 data. The (d) shear modulus, (e) stress-at-break and (f) strain-at-break values are shown. (g) Representative cyclic tensile data are shown for the CS-1-D film and compared to those from the CS-0 and CS-1 films. The (h) residual strain values and (i) energy recovery values measured at each final tensile strain from (f) are shown.

(Fig. 6f) value has increased greatly. The latter result implies that the Stage II reaction enables improved energy dissipation. Hence, the Stage II *only* process results in permanent crosslinks (from BDDE) as well as H-bonding crosslinks (from residual COOH) at an optimum ratio to provide increased stretchability.

Cyclic tensile data were also obtained (Fig. 6g). The residual strain (Fig. 6h) for CS-0 + BDDE is significantly higher than that for the CS-1 film at all the applied strains, while the energy recovery (~35%) is much lower than that of CS-1 (Fig. 6i). Importantly, these data show that using only the Stage II reaction does not provide the complete change from dissipative to predominantly elastic mechanical properties observed for the Stage I + II CS-1 film as evidenced by the comparison in Fig. 6h and i. Hence, it is only by using the complete Stage I + II process (two-stage BDDE reaction, Scheme 1) that the nanoparticle films can fully transition from a dissipative CS-0 film to a predominantly elastic CS-1 film with almost 100% energy recovery. There appears to be a synergistic process requiring both Stage I and II processes for complete mechanical property transformation.

We note that the discussion above assumed that BDDE was bifunctional and formed crosslinks between –COOH groups. This assumption was tested by replacing BDDE with the mono-epoxide species butyl glycidyl ether (BGE), as discussed in Additional Note 3 and depicted in Scheme S2.† BGE was reacted with the CS-0 dispersion using the Stage I + II method. This system is denoted as CS-0-BGE. Variable pH DLS data and titration data are presented in Fig. S10† whilst SEM data are shown in Fig. S11.† The CS-0-BGE films became brittle and fragmented when placed in $CHCl_3$ (Fig. S12†), implying little, if any, permanent crosslinking. The T_g determined from DMA data (Fig. S13a†) was 44 °C. Tensile data are shown in Fig. S13.† The modulus and stress-at-break values were both lower than those for CS-0 (Table S2†). The cyclic tensile data (Fig. S13f†) showed strong dissipative behaviour with relatively high residual strain (Fig. S13g†), poor energy recovery (28%, Fig. S13h†) and no evidence of significant elasticity. These dissipative behaviours are expected for a ring-opening reaction of CS-0 with a mono-functional epoxide (BGE) because no covalent crosslinking should have been added. The data contrasted with CS-0.5 and CS-1 which were both much more

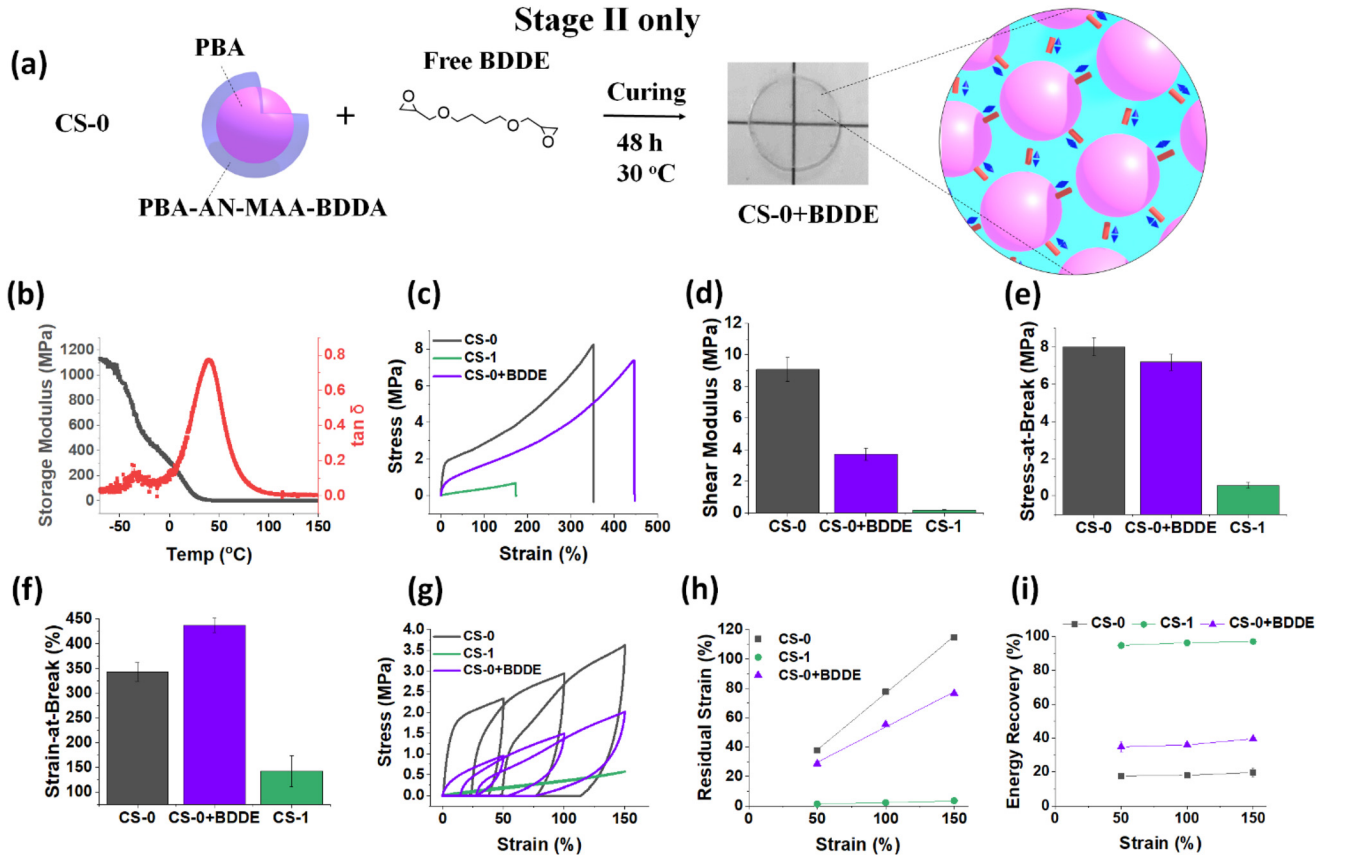

Fig. 6 (a) Depiction of the formation of CS-0 + BDDE films where the CS-0 dispersion is mixed with free BDDE prior to film formation. The CS-0 + BDDE films were prepared using only the Stage II reaction with BDDE. (b) Variation of E' and tan δ with temperature measured for the Stage I CS-0 + BDDE film. (c) Representative stress–strain curve of CS-0 + BDDE compared to CS-0 and CS-1 data (Stage I + II). The (d) shear modulus, (e) stress-at-break and (f) strain-at-break values are shown. (g) Representative cyclic tensile data are shown for the CS-0 + BDDE film and compared to those from the CS-0 and CS-1 films. The (h) residual strain and (i) energy recovery measured at each strain are also shown.

elastic (80% and 97% energy recovery respectively). This comparison confirms that BDDE reacted as a bifunctional crosslinker. It is noted that the modulus, strain-at-break and stress-at-break values for the CS-0-BGE system are all higher than the values for the CS-0.5 and CS-1 films. As discussed in Additional Note 3,† we speculate that these differences originate from the spatial constraints of a difunctional monomer reaction. Briefly, the two epoxy groups of BDDE must react in the same location, whereas BGE is not constrained in this way. Accordingly, we propose that more inter-chain hydrogen bond pairs can occur for the BGE films compared to the BDDE films.

Conclusions

We have introduced a facile new water-based method for the more environmentally friendly synthesis of CS nanoparticle films with highly tuneable mechanical properties. The films can be changed from a dissipative, high modulus system (CS-0, 9.0 MPa, 20% energy recovery) to a lower-modulus, elastic system (CS-1, 0.20 MPa, 97% energy recovery) simply using low-temperature di-epoxide crosslinking. Intermediate compositions contain a tuneable mixture of dynamic and covalent bonding. The CS-0.5 film suggests to be the most improved elastic material with a modulus of 0.40 MPa and energy recovery of 80% while it retains an impressive strain-at-break of more than 300%. This value can be increased to greater than 450% using a monofunctional epoxide (BGE). This tuneability comes about from the decrease of dissipative –COOH crosslinks, decrease in the T_g, and introduction of covalent crosslinks. The CS-0.5 film is a softer and more elastic material with decreased water and $CHCl_3$ swelling compared to the CS-0 films. CS-0.5 may have potential utility where moderate stiffness, high stretchability, energy recovery and/or solvent resistance are required. These may include washers, gaskets, sporting equipment, mats, protective clothing, soft actuators and surface coatings.

The reaction between the –COOH groups and BDDE is shown to occur by crosslinking in two stages which is tuneable by the mass of BDDE used or when the BDDE is reacted (in Stage I or Stage II or both). While higher modulus, high strain-at-break films with some elastic behaviours are achievable by just Stage II, it was revealed that the combination of both Stage I + II provides greater mechanical property changes than

Stage I or Stage II individually with greater elasticity. Not only does this novel approach provide highly tuneable mechanical properties, but it is also water-based which may reduce the negative environmental impact of elastomers. The simple approach used to covalently crosslink –COOH-containing nanoparticle films demonstrated here in the case of nanoparticles made of a PBA core and a poly(BA-*co*-AN-*co*-MAA) shell could, in principle, be applied to other water-based nanoparticle systems with accessible carboxylated functional groups, such as carboxylated NBR latex for example.[66]

Author contributions

M. O-R.: Investigation; visualization; writing – original draft. D. R.: Conceptualization; supervision. X. W.: Investigation. S. W.: Resources. S. E.: Validation; writing – review & editing. B. R. S.: Conceptualization; data curation; project administration; supervision; writing – review and editing.

Data availability

The data supporting this article have been included as part of the ESI.†

Conflicts of interest

There are no conflicts to declare.

Acknowledgements

M. O-R. and B. R. S. gratefully acknowledge the financial support from Synthomer for this research.

References

1 R. J. Young and P. A. Lovell, *Introduction to Polymers*, Francis Group, 2011.
2 L. McKeen, in *Effect of Temperature and other Factors on Plastics and Elastomers*, Elsevier, 2008, ch. 5.
3 J. R. Halladay and R. J. D. Vecchio, *Bonding of Elastomers*, De Gruyter, Berlin, 2020.
4 S. Song, H. Hou, J. Wang, P. Rao and Y. Zhang, *J. Mater. Chem. A*, 2021, **9**, 3931.
5 C. Lou, E. Liu, T. Cheng, J. Li, H. Song, G. Fan, L. Huang, B. Dong and X. Liu, *ACS Omega*, 2022, **7**, 5825.
6 Z. Zhang, N. Ghezawi, B. Li, S. Ge, S. Zhao, T. Saito, D. Hun and P. Cao, *Adv. Funct. Mater.*, 2021, **31**, 2006298.
7 Y. Zhu, Q. Shen, L. Wei, X. Fu, C. Huang, Y. Zhu, L. Zhao, G. Huang and J. Wu, *ACS Appl. Mater. Interfaces*, 2019, **11**, 29373.
8 X. Zhu, K. Han, C. Li, J. Wang, J. Yuan, Z. Pan and M. Pan, *ACS Appl. Mater. Interfaces*, 2023, **15**, 19414.
9 Y. Xu, S. Zhou, Z. Wu, X. Yang, N. Li, Z. Qin and T. Jiao, *J. Chem. Eng.*, 2023, **446**, 143179.
10 A. Hanif, T. Q. Trung, S. Siddiqui, P. T. Toi and N. Lee, *ACS Appl. Mater. Interfaces*, 2018, **10**, 27297.
11 M. Bobnar, N. Derets, S. Umerova, V. Domenici, N. Novak, M. Lavric, G. Cordoyiannis, B. Zalar and A. Resetic, *Nat. Commun.*, 2023, **14**, 764.
12 Z. Pei, Y. Yang, Q. Chen, E. M. Terentjev, Y. Wei and Y. Ji, *Nat. Mater.*, 2013, **13**, 36.
13 Z. Xie, B. Hu, R. Li and Q. Zhang, *ACS Omega*, 2021, **6**, 9319.
14 S. Zhang, K. Liu, T. Wu, M. Xu and S. Shen, *J. Phys. Chem. C*, 2020, **124**, 24429–24434.
15 M. J. Gonzalez-Alvarez, J. Paternoga, K. Breul, H. Cho, M. Z. Roshandel, M. Soleimani and M. A. Winnik, *Polym. Chem.*, 2017, **8**, 2931.
16 M. Argaiz, F. Ruiperez, M. Aguirre and R. Tomovska, *Polymers*, 2021, **13**, 3098.
17 R. S. Gurney, A. Morse, E. Siband, D. Dupin, S. P. Armes and J. L. Keddie, *J. Colloid Interface Sci.*, 2015, **448**, 8.
18 C. Guizard, B. Boutevin, F. Guida, A. Ratsimihety, P. Amblard, J. C. Lasserre and S. Naiglin, *Sep. Purif. Technol.*, 2001, **22–23**, 23.
19 S. Debnath, S. Kaushal and U. Ojha, *ACS Appl. Polym. Mater.*, 2020, **2**, 1006.
20 H. Ye, K. Zhang, D. Kai, Z. Li and X. Loh, *Chem. Soc. Rev.*, 2018, **47**, 4545.
21 S. Kim, H. Jeon, S. Shin, S. Park, J. Jegal, S. Y. Hwang, D. X. Oh and J. Park, *Adv. Mater.*, 2018, **30**, 1705145.
22 Y. Cai, L. Yan, Y. Wang, Y. Ge, M. Liang, Y. Chen, H. Zou and S. Zhou, *J. Chem. Eng.*, 2022, **436**, 135156.
23 R. Yang, Y. Yao, Z. Duan, H. Tai, Y. Jiang, Y. Zheng and D. Wang, *Langmuir*, 2020, **36**, 3029.
24 H. Xu, J. Ji, H. Li, J. Tu, Z. Fan, X. Zhang and X. Guo, *Chem. Eng. J.*, 2023, **475**, 146018.
25 Y. Luo, J. Chen, G. Situ, C. Li, C. Zhang, F. Li, C. Li, Z. Luo and X. Zhang, *J. Chem. Eng.*, 2023, **469**, 143958.
26 K. Mantala and D. Crespy, *Macromolecules*, 2023, **56**, 7332.
27 M. Guerre, C. Taplan, R. Nicolay, J. M. Winne and F. E. D. Prez, *J. Am. Chem. Soc.*, 2018, **140**, 13272–13284.
28 S. K. Raut, S. Sarkar, P. Mondal, A. Meldrum and N. K. Singha, *J. Chem. Eng.*, 2023, **453**, 139641.
29 Q. Shi, W. Wu, B. Yu, M. Ren, L. Wu and C. Zhang, *RSC Adv.*, 2022, **12**, 35396.
30 H. Abdeldaim, B. Reck, K. J. Roschmann and J. M. Asua, *Macromolecules*, 2023, **56**, 3304.
31 N. Jimenez, N. Ballard and J. M. Asua, *Macromolecules*, 2019, **52**, 9724.
32 I. Tiggelman and P. C. Hartmann, *Prog. Org. Coat.*, 2009, **67**, 76.
33 P. A. Steward, J. Hearn and M. C. Wilkinson, *Adv. Colloid Interface Sci.*, 2000, **86**, 195.
34 X. Jiang, J. Li, M. Ding, H. Tan, Q. Ling, Y. Zhong and Q. Fu, *Eur. Polym. J.*, 2007, **43**, 1838.

35 F. Lossada, D. Jiao, X. Yao and A. Walther, *ACS Macro Lett.*, 2020, **9**, 70.
36 Y. Liu, Z. Tang, S. Wu and B. Guo, *ACS Macro Lett.*, 2019, **8**, 193.
37 J. Turton, S. Worral, M. S. Musa, A. H. Milani, Y. Yao, P. Shaw, D. Ring and B. R. Saunders, *Polym. Chem.*, 2021, **12**, 466.
38 O. Pinprayoon, R. Groves, P. A. Lovell, S. Tungchaiwattana and B. R. Saunders, *Soft Matter*, 2011, **7**, 247.
39 M. D. Besteti, D. M. G. Freire and J. C. Pinto, *Macromol. React. Eng.*, 2011, **5**, 518.
40 S. Brovellie, R. D. Schaller, S. A. Crooker, F. Garcia-Santamaria, Y. Chen, R. Viswanatha, J. A. Hollingsworth, H. Htoon and V. I. Klimov, *Nat. Commun.*, 2011, **2**, 280.
41 P. Reiss, M. Protiere and L. Li, *Small*, 2009, **5**, 154–168.
42 J. M. Chan, L. Zhang, K. P. Yuet, G. Liao, J. Rhee, R. Langer and O. C. Farokhzad, *Biomaterials*, 2009, **30**, 1627–1634.
43 R. G. Chaudhuri and S. Paria, *Chem. Rev.*, 2011, **112**, 2373–2433.
44 D. Juhue and J. Lang, *Macromolecules*, 1995, **28**, 1306.
45 E. Limousin, N. Ballard and J. Asua, *J. Appl. Polym. Sci.*, 2019, **136**, 47608.
46 R. A. Ramli, W. A. Laftah and S. Hashim, *RSC Adv.*, 2013, **3**, 15543.
47 J. Rosenfeld, F. Ganachaud and D. Lee, *J. Colloid Interface Sci.*, 2024, **653**, 1753.
48 M. S. Musa, A. H. Milani, P. Shaw, G. Simpson, P. A. Lovell, E. Eaves, N. Hodson and B. R. Saunders, *Soft Matter*, 2016, **12**, 8112.
49 S. Tungchaiwattana, R. Groves, P. A. Lovell, O. Pinprayoon and B. R. Saunders, *J. Mater. Chem.*, 2012, **22**, 5840.
50 B. E. Rodriguez, M. S. Wolfe and M. Fryd, *Macromolecules*, 1994, **27**, 6642.
51 O. Pinprayoon, A. Saiani, R. Groves and B. R. Saunders, *J. Colloid Interface Sci.*, 2009, **336**, 73.
52 E. R. Morris, *Carbohydr. Polym.*, 1992, **17**, 65.
53 G. Lee, H. Y. Song, S. Choi, C. B. Kim, K. Hyun and S. Ahn, *Macromolecules*, 2022, **55**, 10366.
54 Y. Zhang, L. Yuan, G. Liang and A. Gu, *ACS Sustainable Chem. Eng.*, 2023, **11**, 9264.
55 Z. Yang, H. Li, Y. Zhong, X. Lai, J. Ding, Z. Chen and X. Zeng, *ACS Appl. Mater. Interfaces*, 2022, **14**, 44878.
56 T. Kimura and M. Hayashi, *J. Mater. Chem. A*, 2022, **10**, 17406.
57 L. Xiao, W. Li, Z. Liu, K. Zhang, S. Li, Y. Wang, J. Chen, J. Huang and X. Nie, *ACS Sustainable Chem. Eng.*, 2022, **10**, 9829.
58 M. Hayashi and R. Yano, *Macromolecules*, 2020, **53**, 182.
59 M. K. Singh and A. Singh, *Characterization of Polymers and Fibres*, Woodhead Publishing, USA, 2022.
60 J. Brandrup, E. H. Immergut and E. A. Grulke, *Polymer Handbook*, John Wiley & Son, New York, 4 edn, 1999.
61 W. Brostow, R. Chiu, I. M. Kalogeras and A. Vassilikou-Dova, *Mater. Lett.*, 2008, **62**, 3152.
62 K. Bandzierz, L. Reuvekamp, J. Dryzek, W. Dierkes, A. Blume and D. Bielinski, *Materials*, 2016, **9**, 607.
63 X. Hu, M. Vatankhah-Varnoosfaderani, J. Zhou, Q. Li and S. S. Sheiko, *Adv. Mater.*, 2015, **27**, 6899.
64 J. Slootman, V. Waltz, J. C. Yeh, C. Baumann, R. Göstl, J. Comtet and C. Creton, *Phys. Rev. X*, 2020, **10**, 041045.
65 Y. Yao, B. Liu, Z. Xu, J. Yang and W. Liu, *Mater. Horiz.*, 2021, **8**, 2742.
66 G. Zhang, H. Feng, K. Liang, Z. Wang, X. Li, X. Zhou, B. Guo and L. Zhang, *Sci. Bull.*, 2020, **65**, 889.